Classical and quantum solutions of the planar accumulation layer problem within the parabolic effective-mass approximation

A. A. Klochikhin,[1,2,*] V. Yu. Davydov,[1] I. Yu. Strashkova,[1] and S. Gwo[3]
[1]*Ioffe Physico-Technical Institute, 194021 St. Petersburg, Russia*
[2]*Nuclear Physics Institute, 188350 St. Petersburg, Russia*
[3]*Department of Physics, National Tsing-Hua University, Hsinchu 300, Taiwan, Republic of China*
(Received 11 July 2007; revised manuscript received 30 October 2007; published 27 December 2007)

Classical and quantum solutions of the planar accumulation layer problem for a degenerate semiconductor within the parabolic effective-mass approximation are presented. The Hartree approximation and the potential theory equation are used to describe the electron-electron and electron-positive charge interactions. Details of the exact analytical solution of the classical Thomas-Fermi equation are presented. The straightforward self-consistent quantum approach is developed. It results in the nonlinear equations similar to that in the quantum field or disordered solid state theories. The nonlinear quantum equations are solved numerically. It has been established that the nanosize accumulation layers containing two two-dimensional-confined bands can be regarded as the most stable states of the inhomogeneous system of such a kind. In the case of inversion layers, the single-band states can be expected to arise. Useful general relations between crystal parameters and confinement energies have been found. The applicability of the quantum solution is demonstrated by using recent literature data obtained by the high-resolution angle-resolved photoemission spectroscopy [L. Colakerol *et al.*, Phys. Rev. Lett. **97**, 237601 (2006)].

DOI: 10.1103/PhysRevB.76.235325 PACS number(s): 71.20.Nr, 73.20.At, 73.61.Ey, 71.18.+y

I. INTRODUCTION

Electrostatic potential that exists near a semiconductor crystal surface has been widely studied theoretically (see, for example, Refs. 1–3). The renewed interest to this problem was stimulated by strong experimental evidences pointing to the existence of an intrinsic electron accumulation layer near the surfaces of the InN and InGaN epilayers.[4–10] Recently, quantization of electrons in InN accumulation layer was directly observed by high-resolution angle-resolved photoemission spectroscopy.[11]

The classical statistical Thomas-Fermi theory is typically used as a background for description of an inhomogeneous electron gas (see, for instance, Ref. 12). The existing theoretical approaches taking into account quantum effects and two-dimensional (2D)-confined states in accumulation layers[1–3] are based on different model approximations of the accumulation layer potential and solution of the linear Schrödinger equation.

Our paper describes the straightforward solution of the classical and quantum problems of the planar accumulation layer for the *n*-type degenerate semiconductor.

We demonstrate that the classical Thomas-Fermi equation in the parabolic band approximation in the low-temperature limit can be solved analytically for a planar accumulation layer of a degenerate semiconductor. This solution gives simple relations between crystal parameters and characteristics of the accumulation layer.

The quantum approach is developed under the assumption that the accumulation layer potential is produced by the external positive charge and by the electrons trapped by 2D bands, while the background free carriers and donor charges screen each other. We neglect, therefore, the possible separation of the background free carriers and positive charges near the surface. This simplification is based on the experimental data[4–10] which show that the concentration of the electrons trapped within accumulation layers of InN samples dominates over the background concentration typically by 2 or 3 orders of magnitude. Under this condition, the influence of the background free carriers and donors can be considered to be negligible. In the case of an inversion layer followed by a depletion layer, the quantum approach developed here becomes exact.

We employ the Hartree approximation and the potential theory to derive the self-consistent equations. In contrast to the previous publications on this subject, we do not use any model presentation of the accumulation layer potential. In the quantum approach, the Schrödinger equation describing the electron motion in the accumulation layer potential should be solved. We show that the Schrödinger equation with the Hartree potential becomes nonlinear and acquires the features of the nonlinear quantum field theory equation. In particular, the amplitude of the wave function plays the role of an important parameter allowing one to proceed to the self-consistent calculations. It is not possible to introduce a similar parameter in the approaches using model potentials and the linear Schrödinger equation. Therefore, it is not possible to reach self-consistency in the framework of a linear approach.

We show that there are two types of the self-consistent quantum solutions which can be used for description of the accumulation layers of the nanoscale size. The first solution contains a single 2D-confined band, while the second one contains two 2D bands. The realization of the second solution appears to be more favorable from the point of view of energy considerations. The single-band solution can, probably, be realized in the case of inversion layers when the electron number is not sufficient to fill the states of the second 2D band.

The theory is developed for the zero temperature limit. This restriction can easily be removed in the quantum ap-

proach by using the temperature dependent Fermi distribution function in all expressions. In the classical solution, where the solution is expressed analytically, this restriction means that the temperature should not influence the electron population of the states below the conduction band bottom, i.e., $kT \ll \mu$, where μ is the electron Fermi level measured from the conduction band bottom.

We present also results of calculations of the accumulation layer characteristics using experimental data of Ref. 11. Despite the fact that our calculations are performed in the parabolic band approximation a good qualitative and quantitative agreement with the experiment is obtained.

II. SOLUTION OF THE CLASSICAL THOMAS-FERMI EQUATION

We consider a typical model of the accumulation layer that arises due to a planar positive charge on the crystal surface. We assume that the semiconductor contains homogeneously distributed donors of density N_D, the charge of which is compensated for by free electrons of density n_e, so that $n_e = N_D$. We neglect, therefore, the spatial fluctuations of the donor density. The planar positive charge of density Q_s is compensated for by additional free electrons $\delta n(z)$ inhomogeneously distributed within the crystal.

The resulting inhomogeneous Coulomb potential, in accordance with the potential theory, can be written as

$$\phi(z) = \int d^2r' dz' \{-Q_s \delta(z')e + \delta n(z')e\} \times \{\varepsilon |(z-z')^2 + (r')^2|^{1/2}\}^{-1}, \quad (1)$$

where $\delta(z')$ is the δ function, the reference point for z is chosen to be at the surface, $\delta n(z')$ is the compensating electron density, and ε is the electron dielectric constant. Neither homogeneous positive donor charge nor homogeneous electron charge contribute to the inhomogeneous potential of the accumulation layer. We consider the potential normalized by the condition

$$\Phi(z) = \phi(z) - \phi(\infty).$$

Then integrating over d^2r' and assuming the electroneutrality

$$Q_s = \int dz \delta n(z), \quad (2)$$

we obtain for the potential

$$\Phi(z) = -\frac{2\pi e}{\varepsilon} \int z' dz' \delta n(z+z'). \quad (3)$$

A similar expression for the potential can be found in Ref. 3. The potential of Eq. (3) satisfies the Poisson equation. The Thomas-Fermi approach assumes that $\delta n(z)$ can be expressed through the Fermi distribution function. Since the surface plane is taken to be isotropic, the potential should have a cylindrical symmetry. Then the Thomas-Fermi equation can be presented as

$$\frac{d^2}{dz^2}[-e\Phi(z)] = \frac{2\pi}{\varepsilon}\frac{e^2}{3\pi^2}\left(\frac{2m^*}{\hbar^2}\right)^{3/2}[-e\Phi(z)]^{3/2}, \quad (4)$$

where m^* is the electron effective mass.

The exact asymptotic for the solution of the Thomas-Fermi equation in the case of spherical symmetry[12] is well known. In the case of a planar accumulation layer the Thomas-Fermi equation is one dimensional, and the exact solution can be obtained in the whole range of z. The potential that is a solution of Eq. (4) is

$$-e\Phi(z) = R_H \alpha \left[\frac{a_B}{z+l}\right]^4, \quad (5)$$

the compensating electron density is

$$\delta n(z) = \frac{10\alpha}{a_B^3}\left[\frac{a_B}{z+l}\right]^6, \quad (6)$$

and the external surface charge density is

$$Q_s = \frac{2\alpha}{a_B^2}\left[\frac{a_B}{l}\right]^5. \quad (7)$$

Here, $R_H = e^2/2a_B$ is the hydrogen Rydberg, $a_B = \hbar^2/m_0 e^2$ is the hydrogen Bohr radius or atomic length unit, and α is expressed via crystal characteristics

$$\alpha = \left[\frac{30\pi\epsilon}{2}\right]^2 \left(\frac{m_0}{m^*}\right)^3, \quad (8)$$

where m_0 is the free electron mass and l is the characteristic length related to the surface charge by Eq. (7). The full electron density in the crystal is given by

$$n(z) = \frac{1}{3\pi^2}\left(\frac{2m^*}{\hbar^2}\right)^{3/2}[\mu - e\Phi(z)]^{3/2}, \quad (9)$$

where μ is the chemical potential which is defined in the limit $z \to \infty$ as

$$\mu = \frac{\hbar^2}{2m^*}(3\pi^2 n_e)^{2/3}. \quad (10)$$

The obtained classical solution gives simple and transparent expressions for the band bending potential and inhomogeneous electron density in terms of crystal parameters and external electrical charge. When the potential of Eq. (5) is found, the electron density for the nonparabolic conduction band can be calculated. Therefore, the nonparabolic dispersion of the electron band in InN can be approximately taken into account.

III. QUANTUM THEORY

A. Quantum confinement in the classical potential

It is convenient to begin the quantum consideration from the solution of the Schrödinger equation with the classical potential of Eq. (5)

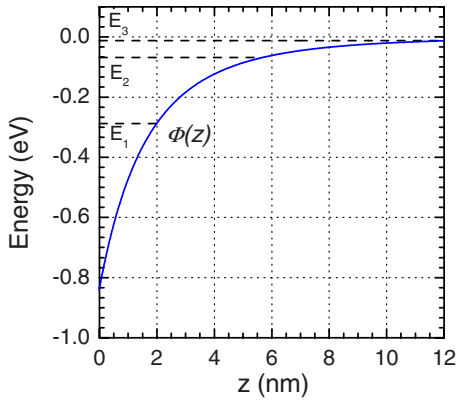

FIG. 1. (Color online) Classical potential $\Phi(z)$ of Eq. (5) of depth 0.84 eV and 2D confinement energies E_i $(i=1,2,3)$ equal to −284, −71, and −11 meV found from Eq. (11) for $\varepsilon=7.16$ and $m^*=0.20m_0$.

$$-\frac{\hbar^2}{2m^*}\frac{d^2\psi_n}{dz^2}+e\Phi(z)\psi_n(z)=\hbar\omega_n\psi_n(z). \tag{11}$$

Here, n enumerates the energies and wave functions of the confined bands. In all quantum calculations we have to separate the potential well and vacuum by a barrier. As an example, Fig. 1 shows results of solution of the Schrödinger equation using the classical potential of Eq. (5). In view of a strong nonparabolic behavior of the conduction band[10] and typically high electron concentrations in InN, we consider high enough value of the effective mass $m^*=0.20m_0$. It can be seen that the potential supports three 2D-confined bands in the accumulation layer at the parameters used.

The 2D-confined bands give the quantum electron density in an accumulation layer

$$\delta n^q(z)=\frac{1}{2\pi}\frac{2m^*}{\hbar^2}\sum_n \hbar\omega_n\psi_n^2(z), \tag{12}$$

where the wave functions are normalized to unity

$$\int \psi_n^2(z)dz=1. \tag{13}$$

Using the atomic length unit

$$z\to x=z/a_B,$$

$$\psi_n^2(z)\to\psi_n^2(x)a_B, \tag{14}$$

we present the electron density as

$$\delta n^q(x)=\frac{1}{a_B^3}\frac{1}{2\pi}\frac{m^*}{m_0}\sum_n\frac{\hbar\omega_n}{R_H}\psi_n^2(x). \tag{15}$$

To derive the potential in the Hartree approximation, we substitute $\delta n^q(z)$ of Eq. (12) and

$$Q_s^q=\int \delta n^q(z)dz$$

into Eq. (1). After integrating over d^2r' we have

$$\Phi_q(z)=-\frac{e}{\varepsilon}\frac{2m^*}{\hbar^2}\sum_n\hbar\omega_n\int\psi_n^2(z+z')z'dz'. \tag{16}$$

According to the potential theory, the potential defined by Eq. (16) satisfies the Poisson equation as well as the initial classical potential. It can be seen, therefore, that the quantum procedure, we are using, does not involve the Poisson equation directly.

Transition to the dimensionless length gives

$$\Phi_q(x)=-\frac{e}{a_B\varepsilon}\frac{m^*}{m_0}\sum_n\frac{\hbar\omega_n}{R_H}\int\psi_n^2(x+x')x'dx'. \tag{17}$$

Therefore, starting from the classical potential of Eq. (5) we obtained the potential of Eq. (17). The results give the band bending and the electron density which differ significantly from the initial classical values. The quantum potential of Eq. (17) and the electron charge of Eq. (15) do not coincide with the initial classical potential of Eq. (5) and classical charge of Eq. (7), respectively. The quantum electron charge $\int\delta n^q(z)dz=3.06\times10^{13}$ cm^{-2} for the potential presented in Fig. 1 is not equal to the classical surface charge $Q_s=3.62\times10^{13}$ cm^{-2}. It is correct to say that the characteristics obtained as the first approximation are not self-consistent.

B. Quantum self-consistent solutions

The aim of the quantum approach is to derive the equation adequate for the procedure of the self-consistent solution of the problem. Substituting the potential of Eq. (16) into the Schrödinger equation, we obtain

$$-\frac{\hbar^2}{2m^*}\frac{d^2\psi_n}{dz^2}+e\Phi_q(z)\psi_n(z)=\hbar\omega_n\psi_n(z). \tag{18}$$

This equation which defines the confinement energies and wave functions becomes nonlinear because $\Phi_q(z)$ is given by Eq. (16). We have taken the reference point for energies at the conduction band bottom (CBB) which is the discrete spectrum boundary.

In contrast to the linear Schrödinger equation [Eq. (11)], where the wave function amplitude can be normalized, the wave function amplitude of nonlinear equation (18) should be found in the process of self-consistent solution of this equation. The nonlinear equation of the Eq. (18) type gives the possibility to perform a self-consistent procedure.

It is convenient to deal with normalized wave functions in calculations by introducing the amplitude $\lambda^{1/2}$

$$\psi_n(z)\to\lambda^{1/2}\psi_n(z). \tag{19}$$

Then the normalized wave function and the amplitude $\lambda^{1/2}$ should be found self-consistently by solving the nonlinear equation

$$-\frac{\hbar^2}{2m^*}\frac{d^2\psi_m}{dz^2}-\frac{\lambda e^2}{\varepsilon}\frac{2m^*}{\hbar^2}\left\{\sum_n\hbar\omega_n\int\psi_n^2(z+z')z'dz'\right\}\psi_m(z)$$
$$=\hbar\omega_m\psi_m(z). \tag{20}$$

We can introduce only one factor λ which is common to the whole expression in the curly brackets of Eq. (20) because

we have to keep the relative contributions of different confined bands into the quantum electron density as they are defined by Eq. (12). The physical meaning of this factor is a renormalization of the dielectric constant of the $\varepsilon \rightarrow \varepsilon/\lambda$ type due to the nonlinear character of the equation.

Using again the dimensionless variable x, we obtain

$$-\frac{\hbar^2}{2m^* a_B^2}\frac{d^2\psi_n}{dx^2} + e\Phi_q^{sc}(x)\psi_n(x) = \hbar\omega_n\psi_n(x), \tag{21}$$

with $\Phi_q^{sc}(x)$ given now by

$$e\Phi_q^{sc}(x) = -\frac{\lambda e^2}{a_B \varepsilon}\frac{m^*}{m_0}\sum_n \frac{\hbar\omega_n}{R_H}\int \psi_n^2(x+x')x'dx'. \tag{22}$$

The self-consistent quantum electron density in an accumulation layer can be written as

$$\delta n_{sc}^q(x) = \frac{\lambda}{a_B^3}\frac{1}{2\pi}\frac{m^*}{m_0}\sum_n \frac{\hbar\omega_n}{R_H}\psi_n^2(x), \tag{23}$$

and the surface charge density following from the self-consistent quantum electroneutrality condition is

$$Q_s^{sc} = \frac{\lambda}{a_B^2}\frac{1}{2\pi}\frac{m^*}{m_0}\sum_n \frac{\hbar\omega_n}{R_H}. \tag{24}$$

Hence, starting from the classical potential of Eq. (5) we obtain the self-consistent equation (21), the solution of which leads to a finite number of confined states. In order to describe the possible quantum self-consistent solutions it is useful to compare the quantum solution of Eq. (11) [using the classical potential of Eq. (5)] with the quantum self-consistent solutions of Eq. (21) [using the quantum potential of Eq. (22)].

The exact solution of the Thomas-Fermi equation gives the short-range potential of Eq. (5), the characteristics of which are defined by the magnitudes of α and l. These parameters are associated with the external charge and crystal constants by Eqs. (7) and (8). The potential of Eq. (5) can support different but finite numbers of localized states depending on the parameters used. The minimal number of localized states in the potential of Eq. (5) is equal to unity, while the maximal number depends on the effective width of the potential well l.

The quantum self-consistent potential of Eq. (22) has the properties that considerably differ from those of the potential of the Thomas-Fermi solution. In order to define the quantum self-consistent potential, we have to choose one of the three following characteristics: (i) its depth, (ii) the depth of the ground localized state, or (iii) the magnitude of the external charge. We also have to choose the number of the terms in the series given by Eq. (22). This number defines the width of the potential well and is a quantum analog of the classical potential width l.

An important property of Eq. (21) is its similarity to the instanton equation[13,14] if the series of Eq. (22) is truncated not only at $n=1$ but also at $n=2$.

This similarity is due to the following: if we preserve only one term in the sum (22), the self-consistent potential supports only one bound state at any value of the parameter (i), (ii), or (iii). In the case two terms in the sum are preserved, the self-consistent potential supports only two bound states at an arbitrary value of one of the parameters [(i)–(iii)].

The situation changes if a third term is included into consideration. The potential (22) supports the higher-order bound states if the sum (22) is truncated at $n=3$. Therefore, the higher-order terms in Eq. (22) should be taken into account. However, if the third and higher terms are included in the self-consistent procedure, the size of the potential well increases sharply up to tens of nanometers, and it is unclear whether the self-consistency can be reached without considering the sample finite thickness or not. This can be explained by the increasing role of the polynomial factors in the wave functions of the third- and higher-order bound states and simultaneous weakening of the exponential factors providing a spatial decay of the wave functions and the potential.

In any case, only two types of self-consistent solutions (single-state and two-state) can be used for the description of a nanoscale accumulation layer. The solutions of Eq. (21) of these two types which we consider below can be classified depending on the number of states.[15]

C. Single-state solutions

The single-state solutions result in the accumulation layers of a minimal thickness and an arbitrary depth. In order to investigate these solutions, it is convenient to use the magnitude of $\sqrt{\hbar/2m^*\omega}$ as the length unit and $\hbar\omega=\hbar\omega_1$ as the energy unit. Then the Schrödinger equation transforms into the dimensionless one similar to the nonlinear equation of the quantum field theory[13,14]

$$-\frac{d^2\psi(y)}{dy^2} - \Lambda\int \psi^2(y+y')y'dy'\psi(y) = \psi(y). \tag{25}$$

This equation has only one confined energy equal to $\hbar\omega$. The dimensionless surface charge density is

$$\Lambda = \frac{2\lambda}{\varepsilon}\left(\frac{R_H}{\hbar\omega}\right)^{1/2}\left(\frac{m^*}{m_0}\right)^{1/2} \approx 1.8. \tag{26}$$

The dimensionless electron charge distribution is

$$\delta n_{sc}^q(y) = \Lambda\psi_n^2(y). \tag{27}$$

The solution of this equation $\psi(y)$ and the magnitude of the dimensional charge density Λ are universal if the barrier restricting the accumulation layer is infinite. In this case a simple scale transformation allows one to obtain a continuous set of solutions with different depths of the potential wells and different confinement energies.

For barriers of finite thicknesses and heights a negligible weak dependence of the accumulation layer on the barrier characteristics appears because of the wave function tail penetration into the barrier.

D. Two-state solutions

A similar transformation of Eqs. (21) and (22) using the dimensionless length and confinement energy units for the case of two-state solutions gives

$$-\frac{d^2\psi_i(y)}{dy^2}-\Lambda_1\int\left[\psi_1^2(y+y')+\frac{\omega_2}{\omega_1}\psi_2^2(y+y')\right]y'dy'\psi_i(y)=\psi_i(y), \tag{28}$$

where $i=1,2$ enumerates the self-consistent wave functions and $\hbar\omega_1$ and $\hbar\omega_2$ are the self-consistent confinement energies. The dimensionless constant Λ_1 is now

$$\Lambda_1=\frac{2\lambda}{\varepsilon}\left(\frac{R_H}{\hbar\omega_1}\right)^{1/2}\left(\frac{m^*}{m_0}\right)^{1/2}. \tag{29}$$

Numerical analysis shows that Eq. (28) does not support the third state. The value of Λ_1 remains ≈ 1.1, and the ratio between the confined energies $\hbar\omega_2/\hbar\omega_1\approx 0.08$ is rather low in a wide range of crystal parameters.

IV. RELATIONS BETWEEN THE SELF-CONSISTENT SOLUTIONS AND THE INTRINSIC CHARACTERISTICS OF AN ACCUMULATION LAYER

A. Theoretical results

The simplest expressions for the accumulation layer characteristics can be obtained in the single-state approximation. The surface charge density is given by

$$Q_s^{sc}=\int\delta n_{sc}^q(x)dx=\frac{\Lambda\varepsilon}{4\pi a_B^2}\left[\frac{m^*}{m_0}\right]^{1/2}\left[\frac{\hbar\omega}{R_H}\right]^{3/2}. \tag{30}$$

This equation relates the observable confinement energy to the most important characteristics of the accumulation layer.

The band bending is equal to $-e\Phi_q^{sc}(0)$ and, therefore, can be presented as

$$-e\Phi_q^{sc}(0)=-\frac{\Lambda e^2}{2a_B}\left[\frac{m^*}{m_0}\right]^{1/2}\left[\frac{\hbar\omega}{R_H}\right]^{3/2}\langle y\rangle, \tag{31}$$

where the dimensionless matrix element of the coordinate $\langle y\rangle$ is of the order of unity. Using an atomic length unit, it can be presented as

$$\langle y\rangle=\int\psi^2(y)ydy=\left(\frac{\hbar}{2m^*\omega a_B^2}\right)^{1/2}\int\psi^2(x)xdx=\left(\frac{R_H}{\hbar\omega}\right)^{1/2}\left(\frac{m^*}{m_0}\right)^{1/2}\langle x\rangle, \tag{32}$$

The matrix element $\langle x\rangle$ is the quantum analog of the classical characteristic length l.

The surface charge density of the two-state solution can be expressed similar to Eq. (30)

$$Q_s^{sc}=\int\delta n_{sc}^q(x)dx=\frac{\Lambda_1\varepsilon}{4\pi a_B^2}\left[\frac{m^*}{m_0}\right]^{1/2}\left[\frac{\hbar\omega_1}{R_H}\right]^{3/2}\left[1+\frac{\omega_2}{\omega_1}\right], \tag{33}$$

and the band bending is

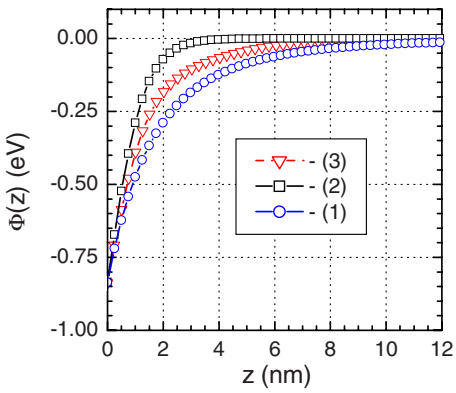

FIG. 2. (Color online) Classical potential and self-consistent potentials of equal depths of 0.84 eV [curves (1) and (2)–(3), respectively]. Curve (2) is the potential of the single-state solution and curve (3) is the potential of the two-state solution. Parameters are $\varepsilon=7.16$ and $m^*=0.2m_0$.

$$-e\Phi_q^{sc}(0)=-\frac{\Lambda_1 e^2}{2a_B}\left[\frac{m^*}{m_0}\right]^{1/2}\left[\frac{\hbar\omega_1}{R_H}\right]^{3/2}\left[\langle y\rangle_{11}+\frac{\omega_2}{\omega_1}\langle y\rangle_{22}\right], \tag{34}$$

if we use $\sqrt{\hbar/2m^*\omega_1}$ as the length unit. Here, $\langle y\rangle_{11}\approx 1$ and $\langle y\rangle_{22}\approx\sqrt{\omega_1/\omega_2}$ are the dimensionless matrix elements of the coordinate for the first and second confined states, respectively. Using the atomic length unit, we transform $\langle y\rangle_{11}\rightarrow\sqrt{\hbar/2m^*\omega_1 a_B^2}\langle x\rangle_{11}$ and Eq. (34) into

$$-e\Phi_q^{sc}(0)=-\frac{\Lambda_1 e^2}{2a_B}\left[\frac{m^*}{m_0}\right]\left[\frac{\hbar\omega_1}{R_H}\right]\left[\langle x\rangle_{11}+\left(\frac{\omega_2}{\omega_1}\right)^{1/2}\langle x\rangle_{22}\right], \tag{35}$$

which demonstrates that the contribution of the second state into the potential is larger than to the surface charge density because of a low ratio $\omega_2/\omega_1\ll 1$.

In Fig. 2 the classical potential is compared with the self-consistent potential wells corresponding to the single-state and two-state quantum solutions. In calculations, equal potential depths were taken. It can be seen that the single-state potential well has the minimal thickness.

In Figs. 3 and 4 the potentials of both quantum solutions are presented together with the positions of the confined levels and squares of the wave functions. It can be seen that the depth of the first confined level of the two-state solution exceeds the depth of the single-state confined energy level.

Figure 5 demonstrates self-consistent confined electron densities for the potential wells presented in Fig. 2. The electron distribution of the single-state quantum solution is narrower than the classical and two-state distributions, while the integral $\int\delta n(z)dz$ is larger for the single-state solution. At the same time, the classical charge for the potential of the same depth is the largest.

Then the question arises which of two quantum solutions will be realized in the case of equal potential well depths. To answer this question we compare full energies of the confined electrons in these two cases. The calculations show that

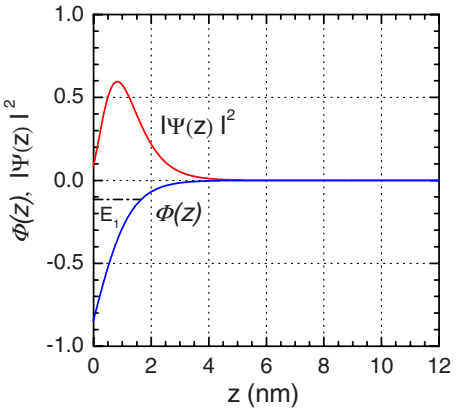

FIG. 3. (Color online) Self-consistent potential of single-state solution, confinement energy, and wave function. The potential depth is 0.84 eV and the barrier height is taken to be 3.4 eV. The parameters are $\varepsilon=7.16$ and $m^*=0.2m_0$. The confined electron content and the quantum surface charge are $\int \delta n(z)dz=Q_s=2.57\times10^{13}$ cm^{-2}. 2D confinement energy is equal to −115 meV.

the full energy is considerably lower for the two-state solution because of a deeper position of the ground confined state. Therefore, the two-state solution is more favorable thermodynamically despite a lower electron content. In the case of equal surface charges Q_s and equal confined electron contents, the potential well will be deeper for the two-state solution, which will lead to a further increase of the depth of the ground confined state and to a lower full energy.

It is worth noting that a single state can be realized for inversion layers. In the case of an inversion layer a decrease in the confined electron content lowers the chemical potential μ below the conduction band bottom. As a result, transformation of $\hbar\omega_1 \rightarrow (\hbar\omega_1-\mu)$ and $\hbar\omega_2 \rightarrow (\hbar\omega_2-\mu)$ in Eq. (28) occurs. This reduces the contribution of the second 2D band into the self-consistent solution and can be followed by a collapse of the two-state solution to a single-state solution

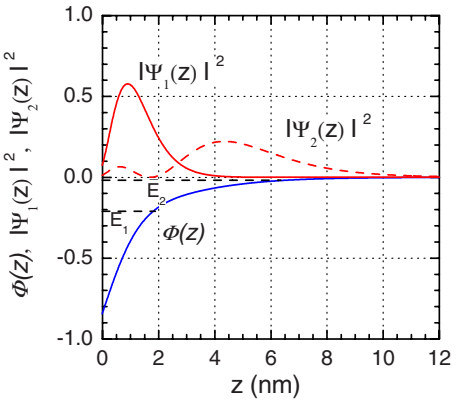

FIG. 4. (Color online) Self-consistent potential, confinement energies, and wave functions of the two-state solution. The potential depth is 0.84 eV and the barrier height is taken to be 3.4 eV. The parameters are $\varepsilon=7.16$ and $m^*=0.2m_0$. The confined electron content and the quantum surface charge are $\int \delta n(z)dz=Q_s=2.09\times10^{13}$ cm^{-2}. 2D confinement energies are equal to −210 and −18 meV.

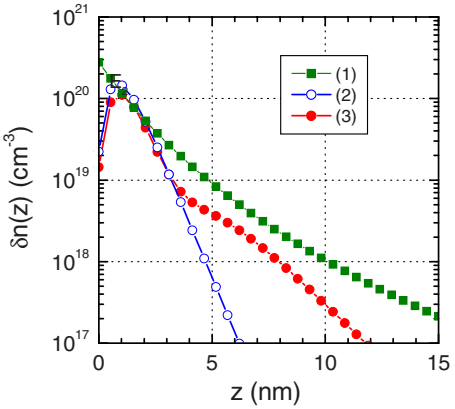

FIG. 5. (Color online) Classical electron density [curve (1)] and self-consistent electron densities [curves (2) and (3)] corresponding to potentials of Fig. 2. Curve (2) is the density of the single-state solution. Curve (3) is the density of the two-state solution. The confined electron contents and the quantum surface charges $\int \delta n(z)dz=Q_s$ for these three densities are 3.62×10^{13}, 2.57×10^{13}, and 2.09×10^{13} cm^{-2}, respectively.

because the two-state self-consistent solution can exist if there are two filled 2D-confined bands.

B. Comparison with experimental data

The applicability of the theory developed was checked in comparison with recent data obtained in the high-resolution angle-resolved photoemission experiment with InN crystals[11] that provided detailed information on the spectra of the 2D states in accumulation layers. We considered the data for the first of the two samples described in this paper.

First of all, we have found that there exists a qualitative agreement between the self-consistent quantum theory and experiment because two confined bands were observed, which is consistent with our quantum theoretical predictions. In order to obtain quantitative estimates, we performed the self-consistent quantum potential calculations for three effective masses $m^*=0.15m_0$, $m^*=0.20m_0$, and $m^*=0.25m_0$. The criterion for fitting was taken to be the depth of the first experimental 2D state. The results are presented in Fig. 6(a). It can be seen that the second 2D states found for the potentials occupy close positions, and the ratio between localization energies is close to $\hbar\omega_2/\hbar\omega_1=0.08$, as it follows from the theory. This ratio agrees well with the experimental data.

We also examine the classical potentials found for effective masses $m^*=0.15m_0$, $m^*=0.20m_0$, and $m^*=0.25m_0$. The potentials were built in such a way that the deepest state energy coincided with the energy of the corresponding experimental state. One of these classical potentials for $m^*=0.20m_0$ is presented in Fig. 6(a). It was found that each classical potential contained three confined bands, which disagrees with the experiment.

Figure 7 presents the detailed comparison of the calculated parabolic and nonparabolic 2D bands with the photocurrent intensity map that reflects the dispersion of quantized states along the $\Gamma\Sigma M$ direction in the surface plane (Fig. 2 of Ref. 11). Note that we used the conduction band bottom

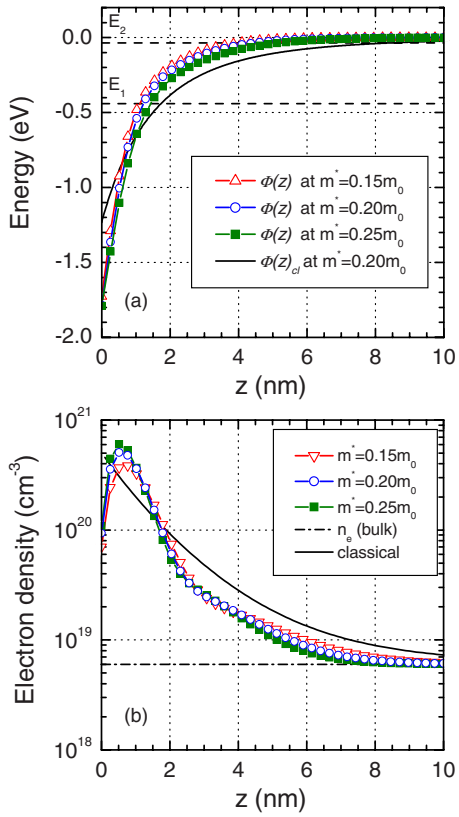

FIG. 6. (Color online) (a) Self-consistent quantum potentials obtained for $\varepsilon=7.16$ and at effective masses $m^*=0.15$, 0.20, and $0.25m_0$, and the classical potential at $m^*=0.20m_0$. The barrier height was taken to be 6 eV. The self-consistent potentials give two 2D-electron bands, the energies of which at zero wave vectors are $E_1=-0.44$ and $E_2=-0.036$ eV. The classical potential supports three 2D states. The deepest of them is at the same energy (≈-0.44 eV) as for the self-consistent potentials, two others at -0.127 and -0.026 eV are not shown. (b) The electron densities corresponding to the potentials of (a). The values of Q_s^{sc} are 5.6, 6.4, and 6.9×10^{13} cm^{-2} for the self-consistent potentials and $Q_s=5.75\times10^{13}$ cm^{-2} for the classical potential. The bulk electron density was taken to be 6×10^{18} cm^{-3}.

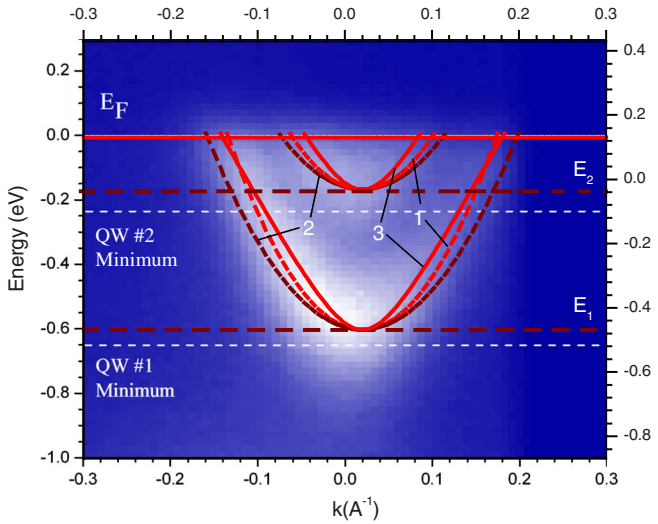

FIG. 7. (Color online). The best fit of the photocurrent intensity map from Ref. 11 by the calculated parabolic and nonparabolic 2D bands. The left energy scale is the original one used in Ref. 11. The energy scale for the calculated energies is shown on the right side of the figure. The reference point is taken to be at the conduction band bottom (CBB) which is the discrete spectrum boundary. Curves (1) and (2) are the 2D-band parabolic dispersions corresponding to effective masses $0.15m_0$ and $0.20m_0$. Curve (3) is the 2D-band nonparabolic dispersion with the effective mass at the Γ point $m_\Gamma=0.07m_0$ and $E_0=0.4$ eV. $E_F=0.130$ eV is the Fermi energy calculated for the nonparabolic dispersion of curve (3) at the electron concentration of 6×10^{18} cm^{-3}. The calculated 2D-electron band energies at zero wave vectors are $E_1=-0.44$ and $E_2=-0.036$ eV.

as the point of reference, while the Fermi energy was used as a reference point in Ref. 11. It can be seen that the experimental results appreciably deviate from the parabolic dispersions corresponding to the effective masses $m^*=(0.15-0.20)m_0$. In order to estimate the role of the nonparabolic deviation in the conduction band dispersion, we performed quantum self-consistent calculations of the potential. In the calculations, the nonparabolic conduction band dispersion was chosen so that it provides the best fit to the data of the photocurrent intensity map (Fig. 2 of Ref. 11). This dispersion (see Fig. 7) was calculated from the expression $\epsilon(k)=\{\sqrt{E_0\hbar^2k^2/2m_\Gamma+E_0^2/4}-E_0/2\}$ that corresponds to a linear increase of the effective mass with kinetic energy[16] $m^*=m_\Gamma(1+E/E_0)$. Here, m_Γ is the effective mass at the Γ point and E_0 is the parameter of the nonparabolic behavior. The Fermi energy corresponding to this dispersion at the electron concentration 6×10^{18} is equal to 0.130 eV. The expression for the potential was found for $m_\Gamma=0.07$ and $E_0=0.4$ eV. Then the self-consistent solution of the Eq. (28) type equation was found. This gives the results for the potential and for the electron density close to those calculated for effective masses $m^*=(0.15-0.20)m_0$ by using the parabolic approximation. The only appreciable difference is a decrease in the $\hbar\omega_2/\hbar\omega_1$ ratio to ≈0.065. Therefore, the nonparabolic dispersion does not lead to radical changes of the results. Note that similar results can be obtained by using the dispersion of the Kane model.[17] More detailed calculations will be given in a separate paper.

V. SUMMARY

To summarize, we have presented classical and quantum solutions of the planar accumulation layer problem for a degenerate n-type semiconductor within the parabolic effective-mass approximation. Details of the exact analytical solution of the classical Thomas-Fermi equation have been given. The classical solution has been used as the zero approximation for the quantum self-consistent calculations. We have shown that there are two types of the self-consistent quantum solutions which can be used for description of accumulation layers of the nanoscale size. The first solution contains a single 2D-confined band, while the second one yields two 2D bands. It has been shown that the solutioncontaining two 2D bands is more favorable from the thermody-

namic point of view. Simple relations between crystal parameters and binding energies have been established. It has been shown that the nonparabolic electron band dispersion does not lead to radical changes in the results obtained. The qualitative and quantitative agreement with experimental data of Ref. 11 is obtained. The self-consistent quantum approach developed in this paper provides a solution of the accumulation layer problem and can be useful in analysis of experimental data.

ACKNOWLEDGMENTS

We are thankful to C. F. McConville for his permission to use Fig. 2 from Ref. 11 and for providing an original version of the figure to us. This work was supported by NSC-RFBR Project 94WFA0400128, Russian Foundation for Basic Research (Grant Nos. 06-02-17240 and 06-02-16218), and the programs "Quantum nanostructures" and "New materials and structures."

*albert.klochikhin@mail.ioffe.ru

[1] C. B. Duke, Phys. Rev. **159**, 632 (1967).
[2] J. A. Appelbaum and G. A. Baraff, Phys. Rev. B **4**, 1235 (1971).
[3] G. A. Baraff and J. A. Appelbaum, Phys. Rev. B **5**, 475 (1972).
[4] Hai Lu, W. J. Schaff, L. F. Eastman, and C. E. Stutz, Appl. Phys. Lett. **82**, 1736 (2003).
[5] I. Mahboob, T. D. Veal, C. F. McConville, H. Lu, and W. J. Schaff, Phys. Rev. Lett. **92**, 036804 (2004).
[6] L. F. J. Piper, T. D. Veal, I. Mahboob, C. F. McConville, H. Lu, and W. J. Schaff, Phys. Rev. B **70**, 115333 (2004).
[7] C. H. Swartz, R. P. Tompkins, N. C. Gilesa, T. H. Myersa, Hai Lu, W. J. Schaff, and L. F. Eastman, J. Cryst. Growth **269**, 29 (2004).
[8] I. Mahboob, T. D. Veal, L. F. J. Piper, C. F. McConville, Hai Lu, W. J. Schaff, J. Furthmüller, and F. Bechstedt, Phys. Rev. B **69**, 201307(R) (2004).
[9] S. X. Li, K. M. Yu, J. Wu, R. E. Jones, W. Walukiewicz, J. W. Ager III, W. Shan, E. E. Haller, H. Lu, and W. J. Schaff, Phys. Rev. B **71**, 161201(R) (2005).
[10] W. Walukiewicz, J. W. Ager III, K. M. Yu, Z. Liliental-Weber, J. Wu, S. X. Li, R. E. Jones, and J. D. Denlinger, J. Phys. D **39**, R83 (2006).
[11] Leyla Colakerol, T. D. Veal, Hae-Kyung Jeong, Lukasz Plucinski, Alex DeMasi, Timothy Learmonth, Per-Anders Glans, Shancai Wang, Yufeng Zhang, L. F. J. Piper, P. H. Jefferson, Alexei Fedorov, Tai-Chou Chen, T. D. Moustakas, C. F. McConville, and Kevin E. Smith, Phys. Rev. Lett. **97**, 237601 (2006).
[12] N. H. March, in *Theory of the Inhomogeneous Electron Gas*, edited by S. Lundqvist and N. H. March (Plenum, New York, 1983).
[13] L. N. Lipatov, Zh. Eksp. Teor. Fiz. **72**, 411 (1977).
[14] E. Brezin and G. Parizi, J. Stat. Phys. **19**, 269 (1978).
[15] A. A. Klochikhin, V. Yu. Davydov, I. Yu. Strashkova, P. N. Brunkov, A. A. Gutkin, M. E. Rudinsky, H.-Y. Chen, and S. Gwo, Phys. Status Solidi (RRL) **1**, 159 (2007).
[16] A. A. Klochikhin, V. Yu. Davydov, V. V. Emtsev, A. V. Sakharov, V. A. Kapitonov, B. A. Andreev, Hai Lu, and William J. Schaff, Phys. Rev. B **71**, 195207 (2005).
[17] E. O. Kane, J. Phys. Chem. Solids **1**, 249 (1957).